

# ANALYTICAL MODELLING OF WIND-VORTEX-INDUCED VIBRATION OF CYLINDERS AND CABLES

Paulo Fernando Villafañe Garcia, [pfvg@hotmail.com](mailto:pfv@hotmial.com)

Francisco Ricardo da Cunha, [fracunha@uol.com.br](mailto:fracunha@uol.com.br) (corresponding author)

Universidade de Brasília, Faculdade de Tecnologia, Departamento de Engenharia Mecânica, Campus Universitário Darcy Ribeiro, 70910-900, Brasília – DF, Brasil

**Abstract.** *In this article we derive the governing differential equations for modelling the unsteady motion of a cylinder suspended by four parallel springs and a cable with pinned ends with both structures under the effects of a cross-flow. A dimensional analysis is used to obtain the level of greatness and influence of the variables involved in the governing equations of a wind-vortex-induced vibratory motion. The relevant physical parameters of the fluid-structure interaction problem examined are the Reynolds number, the anisotropic ratio and the dimensionless frequency. The situations of short and long cables are also identified by means of the dimensional analysis. The nondimensionalized governing equations are solved by using perturbation methods and numerical solutions. Results of the transversal displacement are presented for different Reynolds, anisotropic ratios and frequencies. In addition, experimental measurements of velocity time series by a hot-wire anemometry technique in a wind tunnel are presented. A formal statistical treatment of the velocity signals is performed and a complete nonlinear frequency response for both structures (cylinder and cables), including a resonance analysis is presented for different Reynolds and cable traction.*

**Keywords:** *vortex-induced vibration, perturbation method, vibrating cylinder, oscillating cable, nonlinear frequency response*

## 1. INTRODUCTION

When a fluid flows around a cylinder-shaped body, vortices of intercalated configuration downstream the body are formed. To this phenomenon is given the name of vortex shedding (Batchelor, 1967). The vortices are presented alternately with circulations in both clockwise and anticlockwise directions and are originated periodically. The pressure gradients generated by the vortex shedding induce an alternated force on the body. This force is harmonically variable and perpendicular to the main flow direction. This phenomenon was studied in the past by Kármán, using dimensional analysis on a vibrating cylinder experiment. It was checked the existence of a relation between vortex shedding angular frequency  $\omega_s$ , the cylinder radius  $a$  and the free current velocity  $U$ , being that relation denoted by the Strouhal number  $Sh$ , defined as  $\omega_s a / U$ .

The main goal of this article is the analysis of the vibratory motion of a cylinder and a flexible cable when the resonance phenomenon occurs. That means, when the vibration frequency of the cylindrical body equals or gets close to the vortex shedding frequency. The importance of the resonance is given by the fact that in this state of vibration the highest peak-to-peak amplitudes of the cylindrical body displacement are reached. Consequently it leads to the fracture by fatigue in transmission cables.

In the case of a conduction cable, vibration process by the vortices shedding is more complex. In this case, there is a retroaction between the elastic structure and the air flow by means of a self-damping along the cable. This damping is generated by the friction between the various twisted strings that constitute the cable. When there is resonance, the vibration pattern does not change even with variable wind velocity. The vortex shedding starts being controlled by the vibratory process itself. It is going to be showed later in this article that the cable may have a very dense natural frequency spectrum. This fact raises a lot the chance of the vortex shedding frequency to be equal, or get close, to one of the natural frequencies of the cable, making it to start working in resonance.

## 2. GOVERNING EQUATIONS

### 2.1. Governing equation for cable vibration

First consider the free body diagram of a piece of a cable, as shown in Fig. 1.

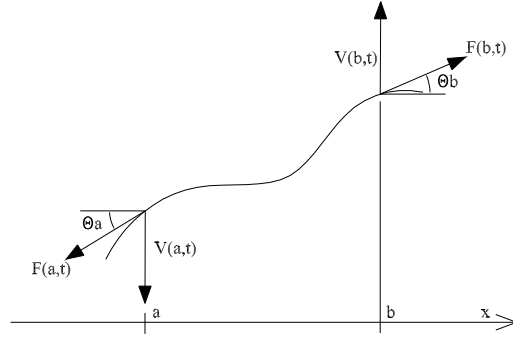


Figure 1. Free body diagram of a non-excited cable

For the governing equation of the vibratory movement of a conduction cable, some hypotheses are taken into account, as it follows:

- The constitutive particles of the cable only have displacement in the  $y$  direction (transversal vibration);
- The conduction cable has constant transversal section, that is, its inertia moment  $I$  does not vary in the  $x$  direction nor with time  $t$ ;
- The conduction cable has constant elasticity module  $E$ , that is,  $E$  does not vary in time nor in space;
- The horizontal force  $T$  is the same force applied to the cable in its ends when they are pinned to poles;
- It is reasonable to assume the  $T$  force invariant over time;
- The cable linear density  $\gamma$  is homogeneous, that is,  $\nabla\gamma = \mathbf{0}$ .

A priori, the linear density  $\gamma$  is a function of  $t$ . However, by the first hypothesis, it is verified that the linear density cannot vary over time.

It is known that the governing equation of a vibrating string is given by (De Figueiredo, 2003):

$$\gamma \frac{\partial^2 y}{\partial t^2} = T \frac{\partial^2 y}{\partial x^2} + F_{ext} \quad (1)$$

where  $F_{ext}$  are all the external forces acting over the string, like the aeolian force and the self-damping force, both presented later. A cable, differently of a string, has flecnional resistance. Under this condition, the sum of the external forces considered in the balance to get the governing equation takes into account the vertical shear forces  $V(x,t)$ . Thus, the governing equation for a cable developing a vibratory motion is given by:

$$EI \frac{\partial^4 y}{\partial x^4}(x,t) - T \frac{\partial^2 y}{\partial x^2}(x,t) + \gamma \frac{\partial^2 y}{\partial t^2}(x,t) = F_{ext}(x,y,t) \quad (2)$$

It is proposed in this article an equation for the external aeolian force per length unit  $F_v$ , transversal to the flow that acts over a cable. This relation is given by a typical hydrodynamic force:

$$F_v = \rho a U^2 C_L \quad (3)$$

where  $\rho$  is the specific mass of the air,  $a$  is the cable radius,  $U$  is the non-disturbed flow velocity and  $C_L$  is the lifting coefficient.

Oliveira and Freire (1994) proposed a fitting equation for the lifting coefficient  $C_L$  based on the equation deductions of Diana and Falco (1971) for a cylinder in vibratory motion. This empirical relation is given by:

$$C_L(\tilde{x}, \tau) = \alpha_1 \delta(\tilde{x}, \tau) + \alpha_2 \delta^2(\tilde{x}, \tau) \quad (4)$$

where  $\delta$  is the nondimensionalized vibration amplitude of the cable,  $\alpha_1$  and  $\alpha_2$  can be determined by means of experimental data,  $\tilde{x}$  and  $\tau$  are nondimensionalized cable-length position and time variables, respectively.

The self-damping force per length unit (equivalent to the viscous damping force of a mass-spring-damper system), was proposed by Diana *et al* (2000) as being:

$$F_a = C(x,t) \frac{\partial y}{\partial t}(x,t) \quad (5)$$

where  $t$  is the time,  $x$  is the position variable along the cable,  $y$  is the cable transversal displacement and  $C(x,t)$  is the cable self-damping coefficient.

## 2.2. Governing equation for cylinder vibration

A simpler system to study and at the same time similar to the cable vibration problem is the concentrated parameters model of a cylinder vibration by the wind. Consider a cylinder of mass  $m_{cil}$  as shown in Fig. 2.

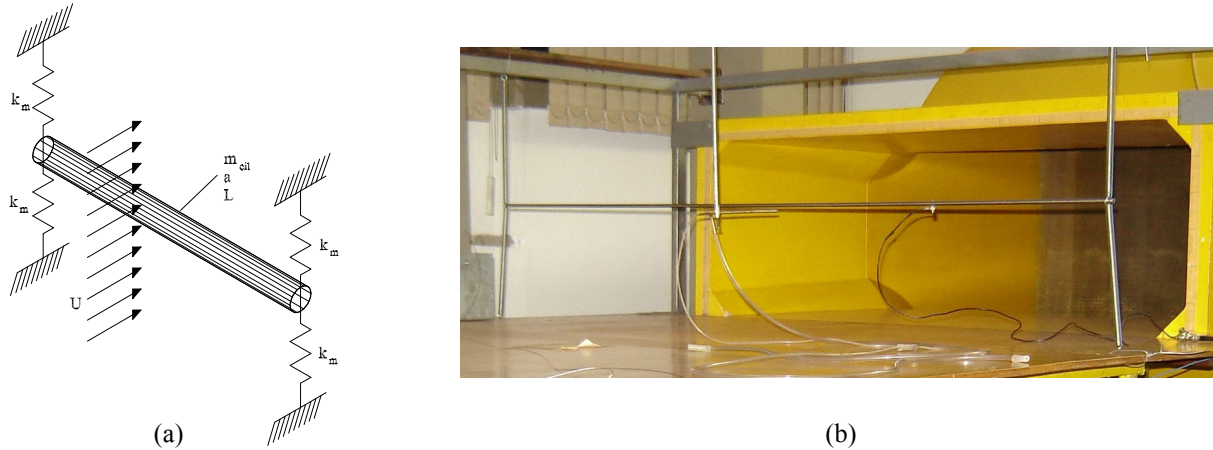


Figure 2. (a) Model of an experimental bench for cylinder vibration experiments, with cylinder aspect ratio  $L/a$  subjected to a transversal wind flow of velocity  $U$ . (b) Photo of the cylinder dynamical system used in the experiments. This experimental setup corresponds to the dynamical model shown to the side.

The governing equation for such system can be deduced from a mass-spring-damper system, of concentrated parameters, with variable external force, given by:

$$m\ddot{y} + C\dot{y} + ky = F(t) \quad (6)$$

where  $m_{cil} = m$ ,  $4k_m = k$  and the system damping coefficient is  $C_{sist} = C$ .

Diana and Falco (1971) made several works on this subject, resulting in an equation that describes well the transversal wind force that acts over a cylinder, namely:

$$F(t) = F_0 \cos(\Omega t + \phi) \quad (7)$$

$F_0$  is the aeolian force amplitude, given by:

$$F_0 = \rho La U^2 C_L \quad (8)$$

where

$$C_L(\tau) = \alpha_0 + \alpha_1 \delta(\tau) + \alpha_2 \delta^2(\tau) \quad (9)$$

The polynomial coefficients also can be determined by experimental data fitting.

## 3. DIMENSIONAL ANALYSIS

### 3.1. Dimensional analysis for cylinder vibration

What follows is the nondimensionalization of all the variables involved in the cylinder vibration problem:

$$\delta = y/a ; \tau = \omega_n t ; \frac{C}{m\omega_n} = 2\zeta ; \omega = \frac{\Omega}{\omega_n} ; \omega_0 = \frac{\omega_s}{\omega_n} \quad (10)$$

where  $\zeta$  is the system damping factor and  $\omega_n$  is the no-damped system natural frequency.

After a few algebraic manipulations, the governing equation for a vibrating cylinder stands as follows:

$$\frac{d^2\delta}{d\tau^2} + 2\zeta \frac{d\delta}{d\tau} + \delta = \left( \frac{\rho L a^2}{m} \right) \left( \frac{\omega_s^2}{\omega_n^2} \right) \left( \frac{U^2}{\omega_s^2 a^2} \right) C_L(\text{Re}, \delta) \cos(\omega\tau + \phi) \quad (11)$$

From Equation (11) three physical parameters of the cylinder oscillatory motion can be identified. The first one is the inertia ratio, the second one is the frequencies ratio and the third one, and more important, is the Strouhal number, which is function of the Reynolds number. Thus, it is expected that the cable vibration problem also can be controlled by similar parameters, or even the same ones.

### 3.2. Dimensional analysis for cable vibration

What follows is the nondimensionalization of all the variables involved in the cable vibration problem. We start defining the following dimensionless quantities:

$$\tilde{x} = x/L ; \delta = y/a ; \tau = \omega_n t \quad (12)$$

where  $\omega_n$  is the free system natural frequency and  $L$  is the cable length.

Now the governing equation may be written in terms of the dimensionless quantities, as follows:

$$\frac{EI}{L^2 T} \frac{\partial^4 \delta}{\partial \tilde{x}^4}(\tilde{x}, \tau) - \frac{\partial^2 \delta}{\partial \tilde{x}^2}(\tilde{x}, \tau) + \frac{\gamma L^2 \omega_n^2}{T} \frac{\partial^2 \delta}{\partial \tau^2}(\tilde{x}, \tau) = \frac{L^2}{aT} [F_v(\tilde{x}, \tau) + F_a(\tilde{x}, \tau)] \quad (13)$$

The coefficient of the fourth order derivative term is a nondimensionalized inertia moment  $I^*$ , defined as:

$$I^* = \frac{EI}{LT^2} = \frac{E}{T} \left( \frac{2a}{L} \right)^2 (2a)^2 \quad (14)$$

It is interesting to notice that, for the inverse aspect ratio  $a/L$  to be of order of an unit, which is the case in beams vibrations and close to cable pins,  $I^*$  has a moderate greatness value, turning the fourth order derivative term to be of great relevance in the governing equation, not being negligible. In the case of having an inverse aspect ratio much lower than the unit, which is the case for long cables,  $I^*$  has a weak greatness value, turning the fourth order derivative term negligible in the Eq. (13). In fact, in real applications, the cable length has an order of  $10^2$  m, the traction force on the cable pins has an order of  $10^4$  N, the elasticity modulus  $E$  of a cable made mostly of aluminum has an order of  $10^{10}$  Pa, and for last the cable inertia moment  $I$  has an order of  $10^{-8}$  m<sup>4</sup>, resulting in a coefficient of order  $10^{-6}$ . In this way, it is reasonable to ignore the fourth order derivative term from Eq. (13) in comparison with the other terms of the governing equation.

It is appropriate to define the dimensionless velocity  $\tilde{c}$ :

$$\tilde{c} = \frac{1}{L\omega_n} \sqrt{\frac{T}{\gamma}} \quad (15)$$

Again, after a few algebraic manipulations, the vibrating cable governing equation reduces to the following dimensionless form:

$$\frac{\partial^2 \delta}{\partial \tau^2} - \tilde{c}^2 \frac{\partial^2 \delta}{\partial \tilde{x}^2} = \frac{1}{\pi} \left( \frac{\rho}{\rho_{cabo}} \right) \left( \frac{1}{Sh^2} \right) \omega_0^2 C_L(\text{Re}, \delta) + \left( \frac{C}{\gamma\omega_n} \right) \frac{\partial \delta}{\partial \tau} \quad (16)$$

Equation (16) is similar to Eq. (11), except for the self-damping term. It shows that the cylinder vibration problem as well as the cable vibration problem are controlled by important and well-known physical parameters of the system.

Solving the Equation (16) in its homogenous form using the variables separation method, it is possible to obtain the cable's non damped free vibration natural frequency, given by:

$$f_n = \frac{n}{2L} \sqrt{\frac{T}{\gamma}} \quad (17)$$

where  $n = 1, 2, 3, \dots$  are the vibration harmonics.

#### 4. SOLUTION FOR THE CYLINDER VIBRATION PROBLEM

Substituting Eq. (9) into Eq. (11) we have:

$$\frac{d^2\delta}{d\tau^2} + 2\zeta \frac{d\delta}{d\tau} + \delta = \varepsilon \omega_0^2 (\alpha_0 + \alpha_1\delta + \alpha_2\delta^2) \cos(\omega\tau + \phi) \quad (18)$$

where

$$\varepsilon = \frac{\rho L a^2}{m S h^2} \quad (19)$$

The governing equation of the vibratory motion of a cylinder, given by Eq. (18), can be solved analytically using the regular perturbation method. It applies because the  $\varepsilon$  coefficient has a small value in most practical cases that is used the cylinder model as a simplification of a real system, for instance, vibration of transmission lines (Oliveira, 1989) and offshore structures. For this matter, this article does not take into account restrict cases with high values of  $\varepsilon$ , where the specific mass of the fluid would be much higher than the vibrating element's.

A resolution of the nonlinear ordinary differential equation by the regular perturbation method consists in determining the solution in a power series form as used by Santos (2005):

$$\delta(\tau) = \delta_0(\tau) + \varepsilon \delta_1(\tau) + \varepsilon^2 \delta_2(\tau) + \dots = \sum_{j=0}^n \varepsilon^j \delta_j(\tau) \quad (20)$$

Substituting Eq. (20) into Eq. (18) and then equating coefficients of like powers of  $\varepsilon$ , it results in the following set of ordinary differential equation (ODE):

$$\begin{cases} \ddot{\delta}_0 + 2\zeta \dot{\delta}_0 + \delta_0 = 0 \rightarrow O(\varepsilon^0) \\ \ddot{\delta}_1 + 2\zeta \dot{\delta}_1 + \delta_1 = \omega_0^2 (\alpha_0 + \alpha_1 \delta_0 + \alpha_2 \delta_0^2) \cos(\omega\tau + \phi) = F_1(\tau, \delta_0) \rightarrow O(\varepsilon^1) \\ \ddot{\delta}_2 + 2\zeta \dot{\delta}_2 + \delta_2 = \omega_0^2 (\alpha_1 \delta_0 + 2\alpha_2 \delta_0 \delta_1) \cos(\omega\tau + \phi) = F_2(\tau, \delta_0, \delta_1) \rightarrow O(\varepsilon^2) \\ \vdots \end{cases} \quad (21)$$

The solution of each equation of the system (21) gives the contributions of the solution in Eq. (20). If  $\varepsilon$  is sufficiently small, which is the case of a cylinder vibratory motion, the term of order  $\varepsilon^2$  and higher can be ignored, generating a solution of order  $O(\varepsilon^1)$ . Thus, for  $\varepsilon \rightarrow 0$ , it is only needed to obtain the solution of the first two equations of the system (21).

The ODE of order  $\varepsilon^0$  is the leading order among all the equations in the system and it represents the damped vibration motion of a cylinder. From this equation it is obtained the free damped system natural frequency. In the case of a system with low damping factor, the resonance frequency of the excited system is approximately equal to the natural frequency of the free damped system.

For the solution of the first homogeneous ODE in system (21), we have the following conditions:

$$\zeta < 1 \Rightarrow \delta_0(\tau) = e^{-\zeta\tau} \left[ A_1 \sin(\sqrt{1-\zeta^2}\tau) + A_2 \cos(\sqrt{1-\zeta^2}\tau) \right] \quad (22)$$

$$\zeta = 1 \Rightarrow \delta_0(\tau) = A_1 e^{-\tau} + A_2 \tau e^{-\tau} \quad (23)$$

$$\zeta > 1 \Rightarrow \delta_0(\tau) = e^{-\zeta\tau} \left( A_1 e^{-\sqrt{\zeta^2-1}\tau} + A_2 e^{\sqrt{\zeta^2-1}\tau} \right) \quad (24)$$

where  $A_1$  and  $A_2$  are constants obtained from the initial conditions of the cylinder motion.

The second ODE of the system has a forcing term  $F_1(\tau, \delta_0)$  that depends of the first ODE solution. From the basic differential equation theory, the second ODE, which is not homogeneous, has a solution as the sum of an homogenous solution and a particular solution,  $\delta_1 = \delta_{1h} + \delta_{1p}$ . The homogenous solution is as similar as the Equations (22) to (24).

Now for the particular solution, we found:

$$\begin{aligned} \zeta < 1 \Rightarrow \delta_{1p}(\tau) = & \frac{e^{-\zeta\tau}}{\sqrt{1-\zeta^2}} \text{sen}(\sqrt{1-\zeta^2}\tau) \int_0^\tau F_1(\tau) e^{\zeta\tau} \cos(\sqrt{1-\zeta^2}\tau) d\tau - \\ & - \frac{e^{-\zeta\tau}}{\sqrt{1-\zeta^2}} \cos(\sqrt{1-\zeta^2}\tau) \int_0^\tau F_1(\tau) e^{\zeta\tau} \text{sen}(\sqrt{1-\zeta^2}\tau) d\tau \end{aligned} \quad (25)$$

$$\zeta = 1 \Rightarrow \delta_{1p}(\tau) = -e^{-\tau} \int_0^\tau F_1(\tau) \tau e^\tau d\tau + \tau e^{-\tau} \int_0^\tau F_1(\tau) e^\tau d\tau \quad (26)$$

$$\zeta > 1 \Rightarrow \delta_{1p}(\tau) = -\frac{e^{(-\zeta-\sqrt{\zeta^2-1})\tau}}{2\sqrt{\zeta^2-1}} \int_0^\tau F_1(\tau) e^{(\zeta+\sqrt{\zeta^2-1})\tau} d\tau + \frac{e^{(-\zeta+\sqrt{\zeta^2-1})\tau}}{2\sqrt{\zeta^2-1}} \int_0^\tau F_1(\tau) e^{(\zeta-\sqrt{\zeta^2-1})\tau} d\tau \quad (27)$$

Using the software Maple 7<sup>®</sup>, it was possible to make plots of the damped resonant ( $\omega_0 = \omega = 1$ ) motion of a typical cylinder for different values of  $\varepsilon$ , as shown in Fig. 3.

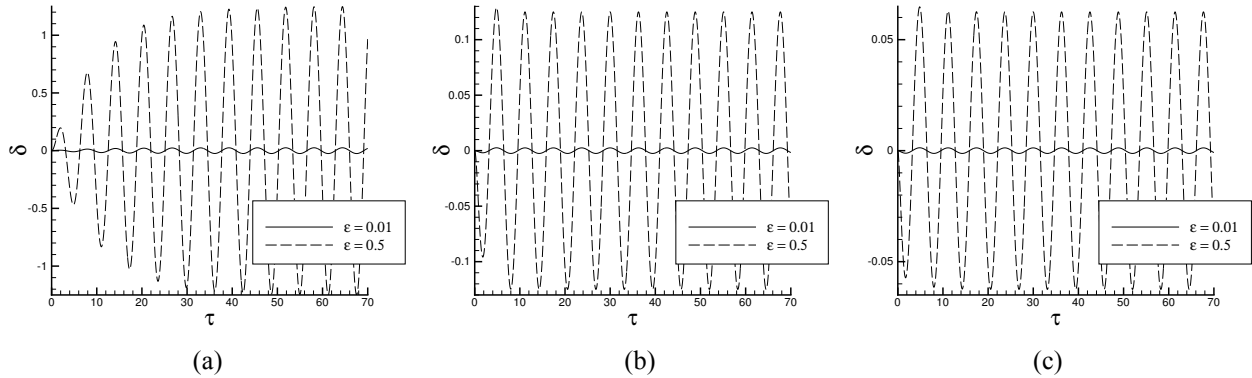
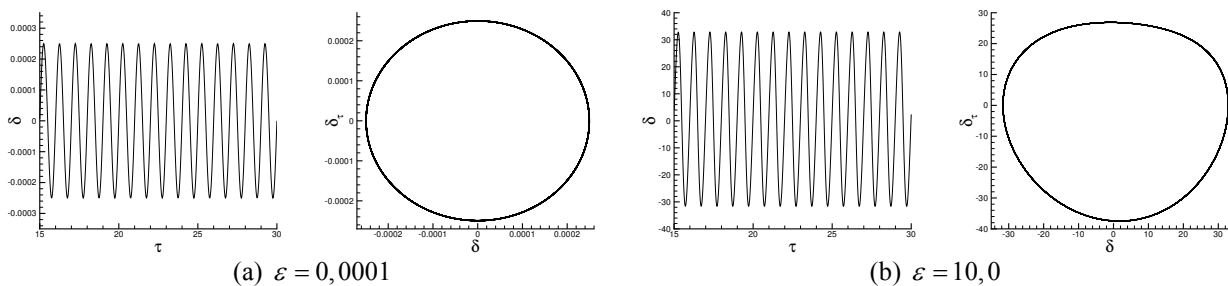


Figure 3. Displacement response of a typical cylinder in resonance for the cases of (a) underdamped system, (b) critical damping and (c) overdamped system.

Solving Equation (18) numerically, using an adaptive time-step fourth-fifth-order Runge-Kutta method and assuming null initial conditions, that is, static cylinder at start, it was possible to plot the resonant displacement time response of the cylinder, in steady state, for the three damping conditions and two distinct values of  $\varepsilon$ . The associate phase diagram  $\delta \times \dot{\delta}$  are also shown in Fig. 4.



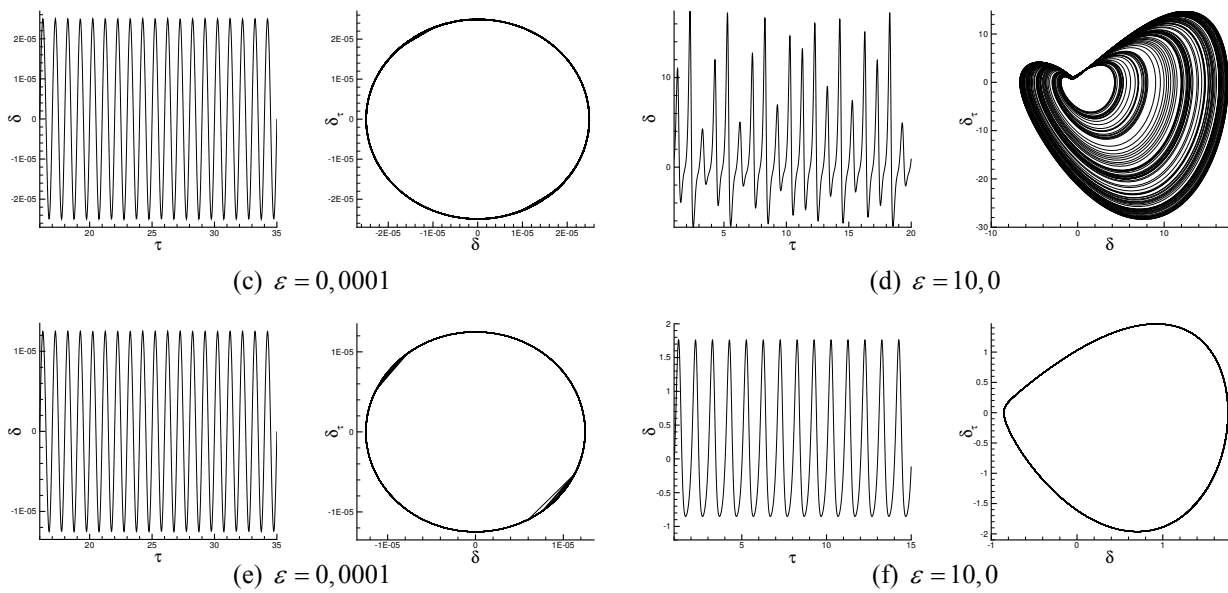


Figure 4. Displacement response and phase diagram of a vibrating cylinder in resonant steady state for (a,b) underdamped, (c,d) critical damping and (e,f) overdamped situations.

It can be observed that as  $\varepsilon$  increases, the nonlinearity in the steady state of the cylinder motion gets more notorious, as shown in the phase diagrams, denoting the decrease in the level of stability of the system. It can also be observed with the increasing of  $\varepsilon$  that the vibration amplitude on the permanent regime increases significantly. For instance, in critical damping vibration (Fig. 4(c) and 4(d)), the amplitude increases in an order of  $10^6$  as  $\varepsilon$  is increased by  $10^5$ .

Increasing  $\varepsilon$  means increasing the air density, increasing the cylinder length, decreasing the cylinder mass or increasing the wind velocity. In an experiment with a wind tunnel size restriction and with not many varieties of fluids, the first two parameters could end up being very hard to be controlled. Thus, in a real experiment, a vibrating cylinder could have a visible vibration steady regime by decreasing its density or increasing the flow velocity in the wind tunnel.

As it can be seen from the plots in Fig. 4, a cylinder does not represent well the vibratory motion of a conduction cable in real application, that is, with low-valued  $\varepsilon$ . In that case, even with the aeolian excitation force being applied continuously, the cylinder tends to stabilize itself in its equilibrium position after a while, but that is the kind of behavior observed in transmission lines. It is expected that the cable, after a while, comes to a permanent regime vibration because of the continuous wind excitation. Anyway, the illustrative response of the cylinder presented above could be expected because of the typically low greatness level of  $\varepsilon$ , which could turn the nonlinear term of the ODE negligible. Thus, the vortex-induced-vibration problem with cylinder could become a simple mass-spring-damper system problem.

Figure 5 compares the maximum displacement in steady state of vibration obtained by numerical and asymptotic solutions for different values of  $\varepsilon$  in the three cases of damping.

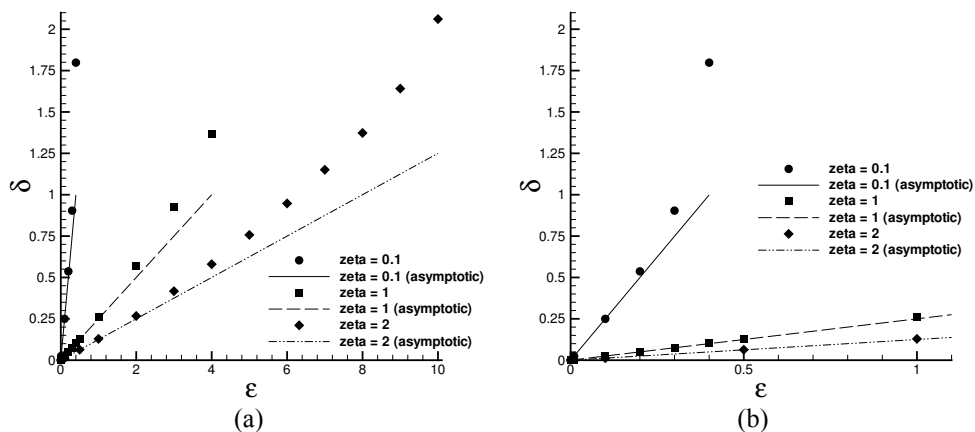


Figure 5. (a) Maximum displacement of the cylinder in steady regime of vibration for different values of  $\varepsilon$ . (b) Zoom of plot for lower values of  $\varepsilon$ .

In Figure 5(a) it is possible to see how the numerical results tend to deviate from the asymptotic solution as  $\varepsilon$  increases, showing for which values of  $\varepsilon$  the numerical solution blows up. For instance, accepting an error around 10%, we found that the numerical model gives acceptable results until  $\varepsilon = 0.2$  for  $\zeta = 0.1$ ,  $\varepsilon = 1$  for  $\zeta = 1$  and  $\varepsilon = 3$  for  $\zeta = 2$ . Nevertheless, the numerical solution works fine for low-valued  $\varepsilon$ , as can be seen in Fig. 5(b), which is a good sign since it shows that the numerical solution gives trustable results for most practical cases in engineering.

## 5. EXPERIMENTAL ANALYSIS

### 5.1. Cylinder vibration

In this work, experiments were done with a stainless steel hollow cylinder suspended by four parallel springs which were mounted on an atmospheric wind tunnel, just as showed on Fig. 2(b). Making use of a hot-wire anemometer, in which sensor was positioned downstream the cylinder, it was captured the temporal series of flow velocity fluctuations. Using the same stochastic treatment made by Oliveira *et al* (2005), it was possible to obtain the power spectra of the velocity fluctuations from undisturbed flow Reynolds number varying from 900 to 4000, as shown in Fig. 6.

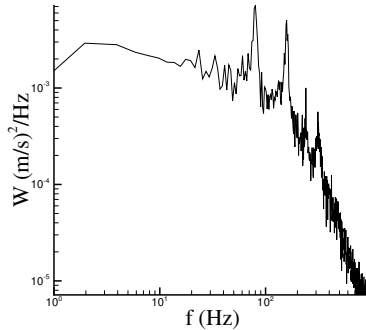


Figure 6. Power spectrum of fluctuation velocity obtained for  $Re = 900$ .

From the power spectrum obtained for each velocity (or Reynolds number) in log-log plot, it was possible to detect two frequencies in which the power dissipated by the flow is maximum, indicating vortex generation. It was evidenced that the second frequency of each power specter, which is the double from the first one, corresponded to a harmonic. More precisely, the second frequency indicates the emission of a vortex that precedes a second one, with the same emission frequency as the first one shown in the specter plot.

In the same experiment, an accelerometer was attached to the cylinder so it was possible to obtain the amplitude fluctuations of the vibrating cylinder. The amplitude capture was done at the same time of the velocity fluctuations data recording.

Having at hand the means of the vibration amplitudes obtained by the accelerometer, the Reynolds numbers for the undisturbed flow and the highest vortex shedding frequencies obtained from the power spectra, plots of the nondimensionalized amplitudes versus Reynolds numbers and nondimensionalized vortex shedding frequencies were made, in order to obtain the laws for the cylinder vibration problem. Those plots are shown in Fig. 7.

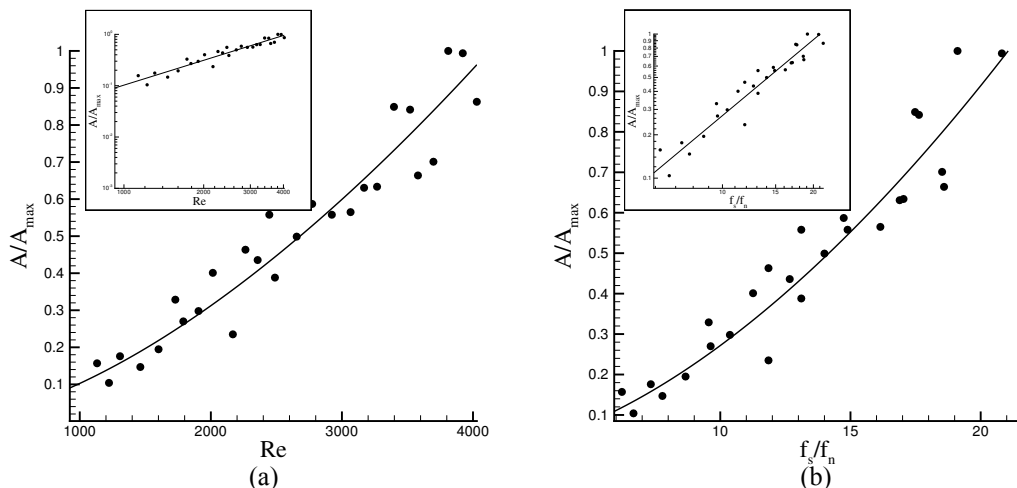


Figure 7. Plots of the cylinder vibration amplitude as function of  $Re$  and  $f_s$ . Inserts show the plots in log-log scale.

Both plots in Fig. 7 show that the amplitude increases with  $Re$  and  $f_s/f_n$ , following closely to a power law. The power laws obtained are respectively:

$$\frac{A}{A_{\max}} = \frac{1}{10} + 2 \times 10^{-6} Re^{5.8} \quad (28)$$

$$\frac{A}{A_{\max}} = \frac{1}{10} + 5 \times 10^{-3} \left( \frac{f_s}{f_n} \right)^{7.4} \quad (29)$$

## 5.2. Cable vibration

For a vibrating thin aluminum cable, the experiments were carried out with the cable pinned at both ends, with one end receiving a variable traction force. While the cable was vibrating for different Reynolds numbers, the traction force was being discretely varied from 1.0 N to 10.0 N for each undisturbed flow velocity.

From the obtained vortex shedding frequencies, it was possible to make Table 1, which relates the vortex shedding frequencies  $f_s$  with the variable traction force  $T$  and the Reynolds number  $Re$  of the flow.

Table 1. Relation of the vortex shedding frequency with the traction force and  $Re$ .

		$Re$							
		132	162	175	187	209	229		
$f_s$ (Hz)		501.9	578.1	642.5	720.5	738.2	728.5	<b>1.0</b>	$T$ (N)
		531.2	607.4	644.5	724.6	730.5	810.5	<b>2.0</b>	
		531.2	562.5	632.8	695.3	726.5	835.9	<b>3.0</b>	
		523.4	597.6	650.4	691.4	724.6	777.3	<b>4.0</b>	
		515.6	574.2	648.4	724.6	712.9	800.8	<b>5.0</b>	
		519.5	585.9	623.0	669.9	728.5	781.2	<b>6.0</b>	
		500.0	599.6	605.4	667.9	765.6	757.8	<b>7.0</b>	
		515.6	578.1	673.8	689.4	744.1	802.7	<b>8.0</b>	
		500.0	587.9	619.1	683.5	751.9	794.9	<b>9.0</b>	
		513.6	560.5	613.3	687.5	746.1	779.3	<b>10.0</b>	

Table 1 shows a tendency of the vortex shedding frequencies to increase as the Reynolds number also increases, just like happened in the cylinder experiment. This tendency is better sketched in the Fig. 8(a), in which  $f_s$  is nondimensionalized by the highest vortex shedding frequency captured by the anemometer. On the other hand, Figure 8(b) shows a decreasing tendency of the flow's dissipating power as  $Re$  increases.

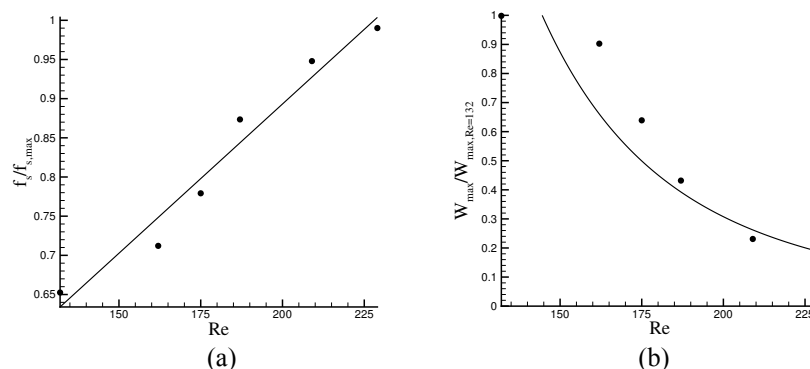


Figure 8. Plots of (a) vortex shedding frequency and (b) dissipating power as a function of  $Re$  for a typical traction.

It was noticed that the vortex shedding frequency increased linearly with  $Re$  at a mean rate of 3.5 for every traction force applied in the experiments. As for the dissipating power of vortex generation, it was found a power law of the type  $W_{\max} = aRe^b$ , where  $b$  is around 3.5 and  $a$  has a specific value for each traction force used in experiments.

Comparing the natural frequency band calculated from Eq. (17) with the vortex shedding frequencies obtained for each traction force applied to the cable, it is possible to create a histogram showing the number of resonant frequency modes as a function of the traction force applied. The histogram is presented in Fig. 9.

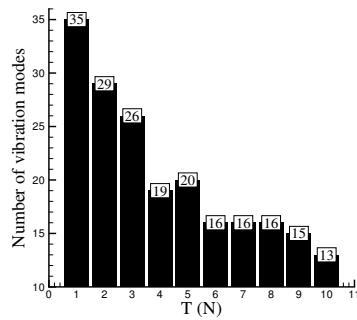


Figure 9. Histogram relating quantity of resonant frequency modes with traction forces.

From a practical point of view, the vibration mode of a cable is determined by the geometric and dynamical characteristics of the system and is also characterized by a specific vibration frequency. By the time of the installation of a transmission line, the technician indirectly determines the cable's vibration modes, or frequency band, by choosing the cable length, the traction force at the pins, the cable material, among other factors. From an analysis of Figure 8 and 9, it is possible to come to the conclusion that it would be better for the cable not to vibrate in the modes which its frequency band coincides with the resonant frequency band, in order to avoid possible fatigue fracture.

## 6. CONCLUSIONS

The presented work has been focused firstly on the nondimensionalization of the governing equations for both cylinder and cable vibration problems. The cylinder vibration problem was analyzed by using a regular perturbation method in order to solve the governing equation and by plots of time responses of a typical cylinder for different values of the weak-term constant  $\varepsilon$ . Those results have shown that a cylinder can have a balanced pattern of vibration for small values of  $\varepsilon$ , but this balance is lost once  $\varepsilon$  is increased, that means, a possible high order of nonlinearity in this fluid-structure problem may cause the structure to eventually collapse. From the experimental results, it was possible to obtain power laws that relate the amplitudes of vibration with the vortex shedding frequency and Reynolds number.

In the final part of this work, the undamped free vibration natural frequency band was compared to the vortex shedding frequencies obtained by the hot-wire anemometer in order to identify resonant patterns. It was possible to conclude that there is an inverse relation between the traction force at the pins of the cable and the number of vibration modes which vibration frequencies are included, entirely or partially, in the system's resonance frequency band.

## 7. ACKNOWLEDGEMENTS

We thank professors Aldo de Sousa and Taygoara de Oliveira for valuable suggestions when preparing this work.

## 8. REFERENCES

- Batchelor, G.K., 1967, "An introduction to fluid dynamics", Cambridge University Press, Cambridge.
- De Figueiredo, D.G., 2003, "Análise de Fourier e equações diferenciais parciais", Ed. Edgard Blucher, S. Paulo, Brazil, 274 p.
- Diana, G. and Falco, M., 1971, "On the forces transmitted to a vibrating cylinder by a blowing fluid", *Meccanica*, Vol. VI, No 1, pp. 9-22.
- Diana, G., Falco, M., Cigada, A. and Manenti, A., 2000, "On the measurement of over head transmission lines conductor self-damping", *IEEE Transactions on Power Delivery*, Vol. 15, No 1, pp. 285-292.
- Oliveira, A.R.E., 1989, "A mathematical model for wind-induced oscillations of cylindrical structures", VI International Conference on Numerical Methods in Laminar and Turbulent Flow, Swansea, Wales, U.K.
- Oliveira, A.R.E. and Freire, D.G., 1994, "Dynamical modelling and analysis of aeolian vibrations of single conductors", *IEEE Transactions on Power Delivery*, Vol. 9, No 3, pp. 1685-1693.
- Oliveira, T.F., Cunha, F.R. and Bobenrieth, R.F.M., 2005, "A stochastic analysis of a nonlinear flow response", *Probabilistic Engineering Mechanics* 21 (2006), pp. 377-383.
- Dos Santos, R.A.M., 2005, "Comportamento dinâmico de bolhas em fluidos complexos", Master's thesis, DM-085, Universidade de Brasília, Brasília, Brasil.

## 9. RESPONSIBILITY NOTICE

The authors are the only responsible for the printed material included in this paper.